ECS Journal of Solid State
Science and Technology

OPEN ACCESS

Microwave Dielectric Properties of the Binary System $BiNbO_4$–$FeNbO_4$

To cite this article: S. Devesa *et al* 2020 *ECS J. Solid State Sci. Technol.* **9** 093010

ECS Journal of Solid State Science and Technology, 2020 **9** 093010

Microwave Dielectric Properties of the Binary System $BiNbO_4$–$FeNbO_4$

S. Devesa,[1,2,z] M. P. Graça,[2] and L. C. Costa[2]

[1]*CFisUC, Physics Department, University of Coimbra, Rua Larga, 3004-516 Coimbra, Portugal*
[2]*I3N and Physics Department, University of Aveiro, 3810-193 Aveiro, Portugal*

The microwave dielectric properties of $BiNbO_4$–$FeNbO_4$ ceramics prepared by the conventional solid-state reaction method, and co-fired at low temperature, had been investigated. The structure, phase composition and surface morphology were studied by X-ray diffraction and scanning electron microscopy techniques, respectively. The dielectric properties of the prepared samples were determined at ≈2.8 GHz, using the modified resonant cavity perturbation method, which accuracy was previously studied using typical cylindrical samples of polytetrafluorethylene. The experimental dielectric constant values of the samples were then fitted to the theoretical curves of different mixture laws.

 [DOI: 10.1149/2162-8777/abb193]

Manuscript submitted July 8, 2020; revised manuscript received August 21, 2020. Published August 31, 2020. *This paper is part of the JSS Focus Issue on 2D Layered Materials: From Fundamental Science to Applications.*

In the last decades, the microwave dielectric ceramics have been extensively used in resonators, filters, radars and integrated passive modules for wireless communication applications.[1,2]

More recently, with the development of commercial wireless technologies, particularly the fifth generation of wireless communications (5 G), the Internet of Things (IoTs) and the military radar systems, the operating frequencies are being continuously expanded from microwave to millimeter-wave.

To meet the specifications of current and future systems, there is an increasing demand for microwave dielectric materials with low dielectric constant ($\varepsilon' < 10$) for fast signal transmission and minimizing the cross coupling between the substrates and the conductors. Other properties, such as high quality factors, for increasing frequency selectivity, and near-zero temperature coefficient of resonant frequency, for stability, are also essential.[3–6]

Moreover, since it is required that the related microwave electronic components become highly integrative, with enhanced performance and low cost, efforts have been made to develop low-temperature co-fired ceramics (LTCC), which require sintering temperatures under 960 °C.[4,7]

The materials characterization at microwave frequencies is a prerequisite to select suitable materials for a specific application.[8] The dielectric properties of a material quantify how the electromagnetic energy interacts with it and are expressed in the form of a complex number, consisting of a real part (ε', dielectric constant) and an imaginary part (ε'', dielectric losses)[9]:

$$\varepsilon^* = \varepsilon' - j\varepsilon'' \qquad [1]$$

At microwave frequencies (300 MHz–300 GHz), the dielectric constant expresses the ability of a dielectric material to be polarised (or store microwave energy within its structure through polarisation), while the dielectric losses refers to the ability of a material to dissipate and transform the stored electromagnetic energy into heat.[10]

Since the microwave dielectric oxide ceramics have a fundamental role in the development of lightweight circuit components for microwave and millimeter-wave frequencies,[8] in this work the novel $BiNbO_4$–$FeNbO_4$ ceramic binary, with compositions of $(1-x)BiNbO_4$–$xFeNbO_4$ ($x = 0.25; 0.50; 0.75$) was investigated.

The dielectric properties of bismuth-based lead-free compounds, including bismuth zinc niobate, bismuth zinc tantalate, bismuth copper niobate, bismuth magnesium niobate and bismuth iron niobate have been studied, with promising results.[11–16] In particular, the substitution of bismuth by iron, lead to a significant increase of the dielectric constant.[15] Given these previous results and since the main advantage of composites is the ability to tailor materials physical properties for special purposes, the $BiNbO_4$–$FeNbO_4$ binary was developed.[17]

The microwave dielectric properties of the prepared samples were determined at ≈2.8 GHz, using the modified resonant cavity perturbation method, proposed by A. Jha,[18] an approach that enhances the accuracy of the conventional cavity perturbation technique. The experimental dielectric constant values of the mixtures were then compared to the theoretical curves of different mixing rules.

The structural and morphological characterization was performed by X-ray diffraction and scanning electron microscopy, respectively.

Experimental

$(1-x)BiNbO_4$–$xFeNbO_4$ ($x = 0.25, 0.50, 0.75$) ceramics were prepared using the conventional solid-state method from the β-$BiNbO_4$ and $FeNbO_4$ oxides, previously prepared by the sol-gel method and reported in Refs. 19 and 20 respectively. The powders were weighted according to the stoichiometric composition of $(1-x)BiNbO_4$–$xFeNbO_4$, and mixed, in a minor amount of ethanol, in a planetary ball mill (Fritsch-Pulverisette 7.0), at 500 rpm. The mixture was milled for 5 h, with 4 agate balls (10 mm in diameter) as milling media. After drying the obtained mixture at 300 °C for 5 h, in a muffle furnace, the powders were pressed into cylinders (using a steel mould and a uniaxial press) and heat-treated at 700 °C, using a dwell time of 4 h and a heating rate of 5 °C min^{-1}. The cooling process was proportional to the furnace inertia.

The crystal structure and phase(s) of the samples were analyzed using X-ray diffraction Empyrean diffractometer, CuK α, 1.54060 Å. The diffraction patterns were obtained at room temperature in the range of 10°−60° by step counting method (0.02° s^{-1}).

In order to confirm the crystal structure and hence retrieve structural information on these compounds, Rietveld refinement was carried out, using the Rietveld structural refinement software PROFEX.[21]

The bulk density was measured using the Archimedes method in reference to water and the theoretical density was obtained using the following equation[3]:

$$\rho_{th} = \frac{\omega_1 + \omega_2}{\omega_1/\rho_1 + \omega_2/\rho_2} \qquad [2]$$

where ω_1, ω_2, and ρ_1, ρ_2 are the mass fractions and the theoretical density of β-$BiNbO_4$ and $FeNbO_4$, respectively.

[z]E-mail: susana_devesa@hotmail.com

The surface morphology of the sintered samples was observed using a scanning electron microscope TESCAN-Vega III.

The microwave characterization was performed using a rectangular resonant cavity, operating in the TE_{105} mode. The measurements of the shift in the resonant frequency and the change in the quality factor, caused by the insertion of the samples, were made at room temperature, using a network analyzer HP 8753D.

The dielectric constant, ε' and the dielectric losses, ε'', of the samples were determined by the modified cavity perturbation (MCP) technique[18]:

$$\varepsilon' = 1 + 2\left[\left(1 + \frac{\sin(k_x r\sqrt{\pi})}{k_x r\sqrt{\pi}}\right)\left(1 + \frac{\sin(k_z r\sqrt{\pi})}{k_z r\sqrt{\pi}}\right)\left(\frac{V_S}{V_C}\right)\right]^{-1} \times \left(\frac{f_0 - f_S}{f_S}\right) \quad [3]$$

$$\varepsilon' = \left[\left(1 + \frac{\sin(k_x r\sqrt{\pi})}{k_x r\sqrt{\pi}}\right)\left(1 + \frac{\sin(k_z r\sqrt{\pi})}{k_z r\sqrt{\pi}}\right)\left(\frac{V_S}{V_C}\right)\right]^{-1} \times \left(\frac{1}{Q_S} - \frac{1}{Q_0}\right) \quad [4]$$

where $k_x = (m\pi/a)$ and $k_z = (p\pi/c)$ represent the wave numbers along the x- and z-direction, respectively, with m and p representing the number of half wave variations of the electric field along x and z-direction, considering a resonant cavity operating in the TE_{m0p} mode.

V_S and V_C are the volumes of the sample and the cavity, respectively, f is the resonance frequency of the cavity and Q its quality factor, where the indexes 0 and S refer to the empty cavity and loaded with the sample.

Figure 1 shows a cylindrical sample of radius r positioned inside the resonant cavity with the TE_{10p} mode configuration, where a and b are the inner cross-sectional dimensions and c is the length of the cavity.

Results and Discussion

Figure 2 shows the X-ray diffraction patterns and the SEM micrographs (inset) of the precursors used to prepare the samples of the binary system $BiNbO_4$–$FeNbO_4$. In Fig. 1a, the diffraction pattern of the pure phase β-$BiNbO_4$ is consistent with the standard ICDD code 04-013-6357,[22] as well as in Fig. 1b, where, according to the ICDD code 04-009-5798,[23] all the peaks can be assigned to the $FeNbO_4$ phase. Table I shows the distance between adjacent planes in the Miller indexes, d_{hkl}, for the peaks assigned to each phase, estimated by the Rietveld structural refinement software PROFEX.

The SEM micrographs of the precursors show very distinctive morphologies. In the case of the bismuth niobate, the occurrence of coalescence is evident, as the existence of pores. The iron niobate presents particles with different sizes and geometries and the grain boundaries are well defined.

The XRD patterns of the $(1-x)BiNbO_4$–$xFeNbO_4$ (x = 0.25, 0.50, 0.75) samples, hereinafter referred to as S1, S2 and S3, respectively, are shown in Fig. 3a. As one can see, only bismuth niobate and iron niobate were identified, which means that the precursors did not react and a binary system was formed.

The Rietveld refinements simulations, made for the studied samples, allowed the estimation of the mass fractions, ω, and the theoretical density of each phase, which are assembled in Table II, as well as the Rietveld fitting parameters.

Figure 3b shows the measured and the calculated spectrum for the sample S1.

The bulk density, ρ_{exp}, values of $BiNbO_4$–$FeNbO_4$ ceramics vs $\boldsymbol{x}$ are shown in Fig. 4. The bulk density decrease with the $FeNbO_4$ content increase is clearly visible. In the inset, the relation between the relative density and the mass fraction of $FeNbO_4$ is shown.

The theoretical density of the binary, determined using the Eq. 2, the porosity, P, estimated by the Eq. 5,[24] and the volume fraction of each phase, obtained with the Eq. 6[25] are also presented in Table II,

$$P = 1 - \frac{\rho_{exp}}{\rho_{th}} \quad [5]$$

$$V_2 = \frac{\omega_2/\rho_2}{\omega_2/\rho_2 + \omega_1/\rho_1} \quad (V_1 + V_2 = 1) \quad [6]$$

where V_1 and V_2 are the volume fractions of β-$BiNbO_4$ and $FeNbO_4$, respectively.

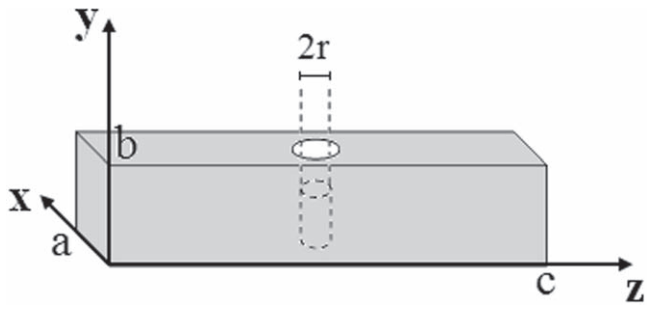

Figure 1. Resonant cavity loaded with a cylindrical sample.

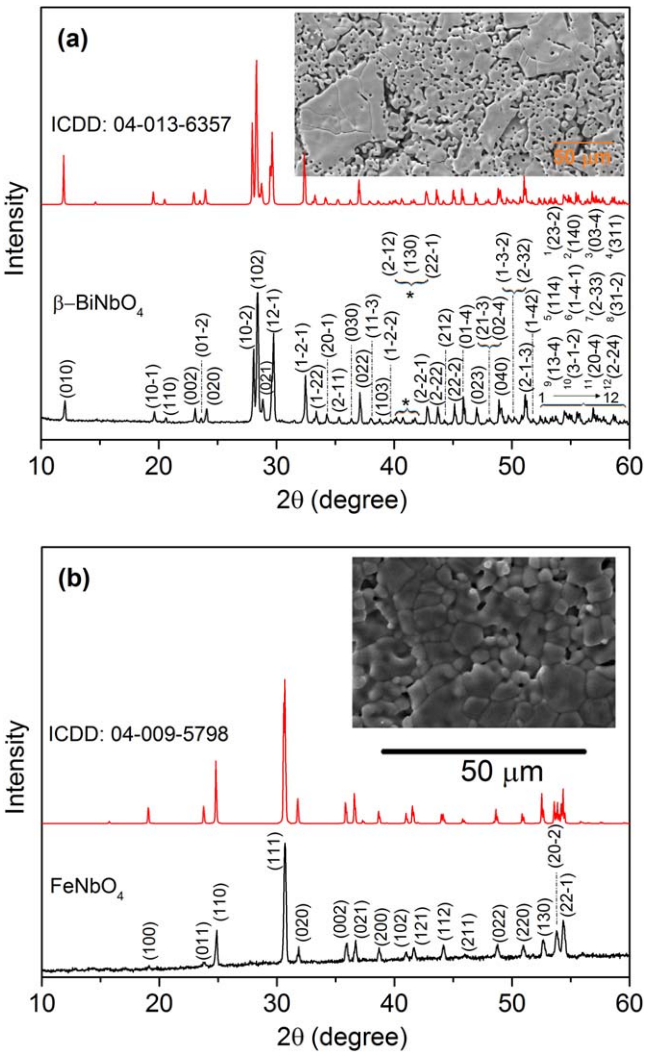

Figure 2. X-ray diffraction patterns and SEM micrographs (inset) of the precursors: (a) β-$BiNbO_4$ and (b) $FeNbO_4$, prepared by the sol-gel method.

Table I. Miller indexes and Bragg positions of the β-$BiNbO_4$ and $FeNbO_4$ peaks.

β-$BiNbO_4$	hkl	0 0 1	1 0 −1	1 1 0	0 0 2	0 1 −2	0 2 0	1 0 −2	1 0 2	0 2 1
	d (nm)	7.7446	4.5325	4.3357	3.8723	3.7874	3.7154	3.1932	3.1533	3.0979
	hkl	1 2 −1	1 −2 −1	1 −2 2	2 0 −1	2 −1 1	0 3 0	0 2 2	1 1 −3	1 0 3
	d (nm)	3.0023	2.7598	2.6926	2.6176	2.5474	2.4769	2.4303	2.3653	2.3277
	hkl	1 −2 −2	2 −1 2	1 3 0	2 2 −1	2 −2 −1	2 −2 2	2 1 2	2 2 −2	0 1 −4
	d (nm)	2.2601	2.2483	2.2195	2.1662	2.1146	2.0754	2.0506	2.0129	1.9815
	hkl	0 2 3	2 1 −3	0 2 −4	0 4 0	1 −3 −2	2 −3 2	2 −1 −3	1 −4 2	2 3 −2
	d (nm)	1.9325	1.8993	1.8937	1.8577	1.8289	1.8176	1.7884	1.7673	1.7483
	hkl	1 4 0	0 3 −4	3 1 1	1 1 4	2 −4 −1	2 −3 3	3 1 −2	1 3 −4	3 −1 −2
	d (nm)	1.7350	1.7169	1.7019	1.6840	1.6695	1.6559	1.6507	1.6292	1.6170
	hkl	2 0 −4	2 −2 4							
	d (nm)	1.5966	1.5722							
$FeNbO_4$	hkl	1 0 0	0 1 1	1 1 0	1 1 1	0 2 0	0 0 2	0 2 1	2 0 0	1 0 2
	d (nm)	4.6525	3.7314	3.5830	2.9090	2.8084	2.4962	2.4477	2.3262	2.198
	hkl	1 2 1	1 1 2	2 1 1	0 2 2	2 2 0	1 3 0	2 0 −2	2 2 −1	
	d (nm)	2.1654	2.0468	1.9729	1.8657	1.7915	1.7369	1.7033	1.6869	

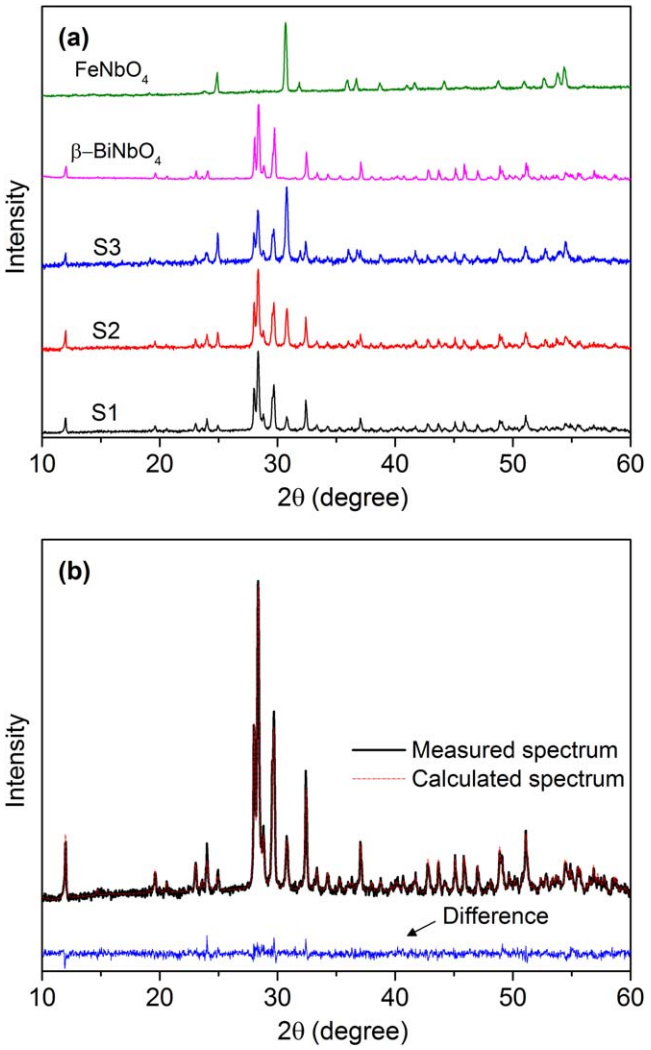

Figure 3. (a) X-ray diffraction patterns of the precursors and studied samples; (b) Measured and calculated spectrum of the sample S1.

The SEM micrographs of the studied samples, presented in Figure 5, were performed with a magnification of 20.0 kx and 40.0 kx (inset).

The images show a morphology completely different from the precursors, with particles with a wide range of geometries and sizes. Nonetheless, it is possible to verify that the number of smaller particles with approximately spherical geometry increases with the increase of the iron niobate content.

Figure 6 shows the transmission of the empty cavity, where a peak can be observed. f_0 is the resonance frequency and $\Delta f_{h/2}$ is the full width at half maximum, FWHM, of the frequency-response curve.

The fundamental concept of the perturbation technique is that the insertion of a dielectric sample in the resonant cavity will cause a shift of the resonant frequency, Δf, for a lower frequency, and a decrease of the quality factor of the cavity, Q, expressed by an increase of the FWHM, as shown in the inset of Fig. 6.

The quality factor can be obtained by the equation[26]

$$Q = \frac{f}{\Delta f_{h/2}} \quad [7]$$

To evaluate the accuracy of the modified cavity perturbation technique, the dielectric constant of typical cylindrical specimens of polytetrafluorethylene, PTFE, was measured and compared with the known dielectric constant, reported as 2.1.[18,27] PTFE was used in this procedure, since its dielectric properties are not temperature and frequency dependent.[28]

Figure 7 shows the dielectric constant of PTFE as a function of the samples radius and, in the inset, as a function of the samples volume. Even for specimens with higher radius and higher volume, this method guarantees the accuracy, with a maximum error of 3.1%.

Figure 8 shows the dielectric constant and the dielectric losses of the studied samples as a function of x. To assure accuracy, all the samples presented radius and volume inferior to 6 mm and 900 mm^3, respectively.

As one can see, with the increase of the iron niobate content, the dielectric constant decreases, with the losses presenting the opposite trend. The increase of the dielectric losses was expected since as the grain size decreases, the increase of the number of grain boundaries per unit volume would result in higher losses.[29]

The theoretical permittivity of $(1-x)BiNbO_4$–$xFeNbO_4$ ceramics, ε'_{mix}, can be estimated by different mixing formulas. The general empirical equations for predicting the dielectric constant of a binary compound are as following[3,4,7,29]:

Parallel mixing model:

$$\varepsilon'_{mix} = V_1\ \varepsilon'_1 + V_2\ \varepsilon'_2 \quad [8]$$

Series mixing model:

$$\frac{1}{\varepsilon'_{mix}} = \frac{V_1}{\varepsilon'_1} + \frac{V_2}{\varepsilon'_2} \quad [9]$$

Table II. Physical parameters of the $BiNbO_4$–$FeNbO_4$ ceramics and Rietveld fitting parameters. [Where ω_1 and ω_2 are the mass fractions, ρ_1 and ρ_2 the theoretical densities V_1 and V_2 the volume fractions, of β-$BiNbO_4$ and $FeNbO_4$, respectively; ρ_{th} and ρ_{exp} are the theoretical and the bulk density of $BiNbO_4$–$FeNbO_4$ ceramics.].

	Physical parameters								
Samples	ω_1 (%)	ω_2 (%)	ρ_1 (g cm^{-3})	ρ_2 (g cm^{-3})	ρ_{th} (g cm^{-3})	ρ_{exp} (g cm^{-3})	P	V_1 (%)	V_2 (%)
S1	80.19	19.81	7.436	5.416	6.924	5.2	0.25	74.67	25.33
S2	59.94	40.06	7.435	5.414	6.468	4.9	0.24	52.14	47.86
S3	33.33	66.67	7.436	5.415	5.954	4.4	0.26	26.69	73.31
Samples	**Rietveld fitting parameters**								
	R_{wp}				R_{exp}			χ^2	
S1	5.27				3.99			1.74	
S2	4.93				3.82			1.67	
S3	4.88				4.02			1.47	

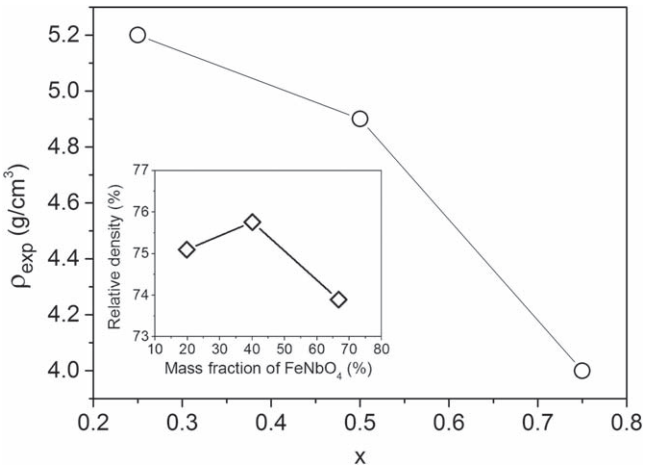

Figure 4. Bulk density as a function of x and relative density as a function of $FeNbO_4$ mass fraction (inset) of the $BiNbO_4$–$FeNbO_4$ ceramics.

Maxwell model:

$$\varepsilon'_{mix} = \frac{V_1\ \varepsilon'_1\left(\frac{2}{3} + \frac{\varepsilon'_2}{3\ \varepsilon'_1}\right) + V_2\ \varepsilon'_2}{\varepsilon'_1\left(\frac{2}{3} + \frac{\varepsilon'_2}{3\ \varepsilon'_1}\right) + V_2} \quad [10]$$

Lichtenecker empirical logarithmic model:

$$\ln\ \varepsilon'_{mix} = V_1\ \ln\ \varepsilon'_1 + V_2\ \ln\ \varepsilon'_2 \quad [11]$$

Jayasundere-Smith model:

$$\varepsilon'_{mix} = \frac{\varepsilon'_2\ V_2 + \varepsilon'_1\ V_1[3\varepsilon'_2/(\varepsilon'_1 + 2\varepsilon'_2)][1 + 3V_1(\varepsilon'_1 - \varepsilon'_2)/(\varepsilon'_1 + 2\varepsilon'_2)]}{V_2 + V_1[3\varepsilon'_2/(\varepsilon'_1 + 2\varepsilon'_2)][1 + 3V_1(\varepsilon'_1 - \varepsilon'_2)/(\varepsilon'_1 + 2\varepsilon'_2)]} \quad [12]$$

where ε_1 and ε_2 are the respective dielectric constants of β-$BiNbO_4$ and $FeNbO_4$ phases, and V_1 and V_2 ($V_1 + V_2 = 1$) are the volume fractions of the corresponding phase.

These models were derived from different assumptions. For a two phase's material, the simplest description is to consider the dielectric as parallel layers of two dielectrics. If the electric field is perpendicular to the plane of the layers, the Eq. 8 applies. Alternatively, if the electric field is parallel to the plane of the layers, the dielectric constant is given by Eq. 9.[29]

A more realistic model, proposed by Maxwell, is presented in Eq. 10. The spherical particle model assumed that the second material consists of spherical particles and these particles are randomly dispersed in the matrix. When the doping concentration is very high, to eliminate the deviation between the experimental results and the Maxwell spherical particle model or the Lichtenecker logarithmic model, Eq. 11, the Jayasundere-Smith model, Eq. 12, considers the impact from surrounding spheres.[1,29]

Figure 9 shows the values of the dielectric constant of $(1-x)BiNbO_4$–$xFeNbO_4$ samples as a function of volume fraction of $FeNbO_4$, estimated by different mixing laws, as well as the experimental data, for comparison. The dielectric properties of β-$BiNbO_4$ and $FeNbO_4$ phases were also determined by the modified cavity perturbation technique, and are presented in Table III.

As one can see, the measured dielectric constants do not agree with the values predicted from the mixing rules. This deviation can be due to the porosity of the samples, and the estimated values can be corrected by applying different approximations.

Considering the parallel mixing model and assuming that phase 1 is the dielectric and phase 2 is the porosity ($\varepsilon' = 1$), Eq. 8 reduces to[29]:

$$\varepsilon'_{corr} = \varepsilon'_{mix} - P(\varepsilon'_{mix} - 1) \quad [13]$$

The dependence of porosity when $0.08 < P < 0.4$ can also be studied by the Maxwell–Garnett formula[4,30]:

$$\varepsilon'_{corr} = \varepsilon'_{mix} + \frac{3P\varepsilon'_{mix}(1 - \varepsilon'_{mix})}{1 + 2\ \varepsilon'_{mix} - P(1 - \varepsilon'_{mix})} \quad [14]$$

Heidinger et al. proposed a equation for spherical pores in a dielectric for cases where $\varepsilon'_{mix} - \varepsilon'_{corr} \ll \varepsilon'_{mix}$[29]:

$$\varepsilon'_{corr} = \varepsilon'_{mix}\left(1 - \frac{3P(\varepsilon'_{mix} - 1)}{2\ \varepsilon'_{mix} + P}\right) \quad [15]$$

The dielectric constant values predicted by the parallel mixing model and corrected by the presented formulas, are presented in Fig. 10. Since the porosity of the studied samples is very similar, for the correction models was considered an average value. As one can see, Eq. 13 provided the best fitting to the measured values.

The quality factor of the binary composite can be estimated by[1,3]

$$\frac{1}{Q} = \frac{V_1}{Q_1} + \frac{V_2}{Q_2} \quad [16]$$

where Q represents the quality factor of the mixture system, and Q_1 and Q_2 are the quality factors of the two ceramics.

Table III shows the quality factors of the β-$BiNbO_4$ and $FeNbO_4$ phases, used to predict the binary quality factor (Eq. 16), Q_{calc}, as well as the experimental quality factor (Eq. 7), Q_{exp}.

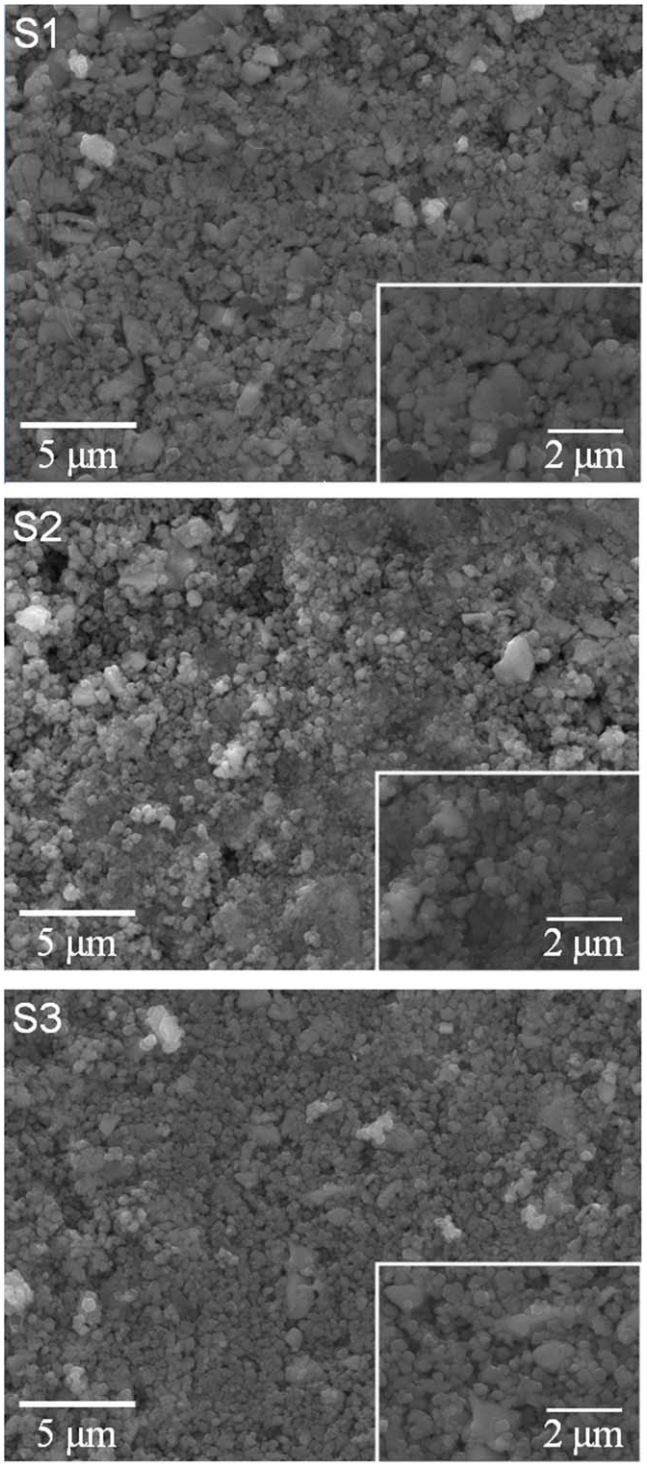

Figure 5. Scanning electron microscopy micrographs of the BiNbO4–FeNbO4 ceramics.

The trend of the calculated results is roughly consistent with the experimental data, however, the values predicted by the mixing law are much higher than the experimental ones. This difference may be due to the porosity, that is not considered by the mixing rules. Besides that, the small grains present in the binary samples increased the number of grain boundaries, which act as defects in crystals, increasing the dielectric losses and decreasing the quality factor.[5]

The obtained results are in agreement with Ref. 1, that claims that Eq. 14 is not a general model, and for that reason, unable to predict the quality factor of all binary ceramic systems.

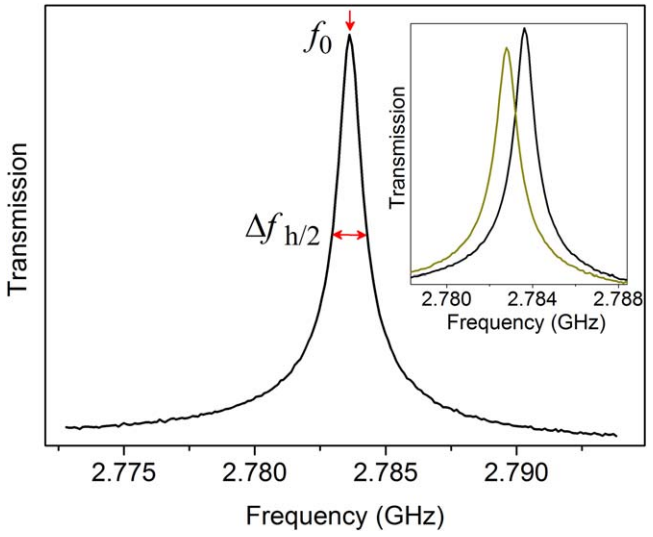

Figure 6. Empty cavity spectrum, highlighting the resonant frequency and the FWHM of the frequency-response curve. Inset: transmission of the cavity, empty and with a sample.

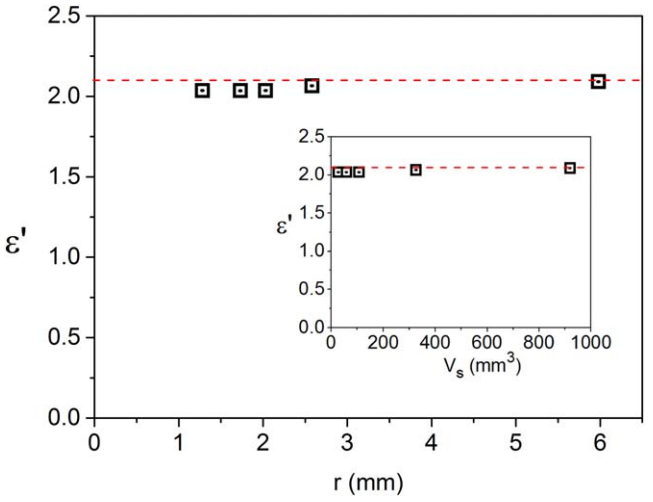

Figure 7. PTFE dielectric constant as a function of the samples radius and volume (inset).

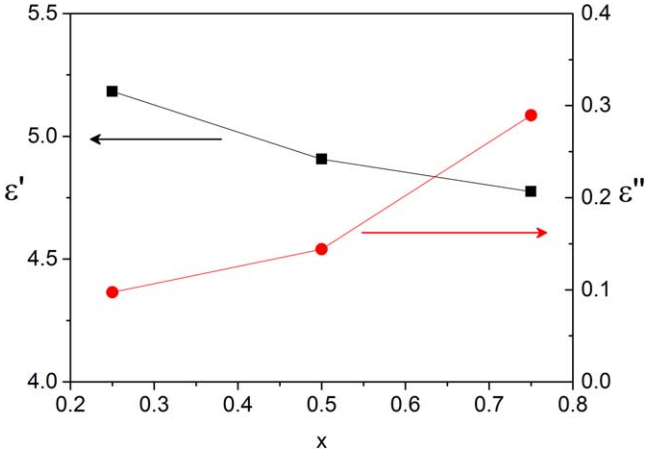

Figure 8. Dielectric constant and dielectric losses of $(1-x)BiNbO_4$–$xFeNbO_4$ ceramics as a function of x.

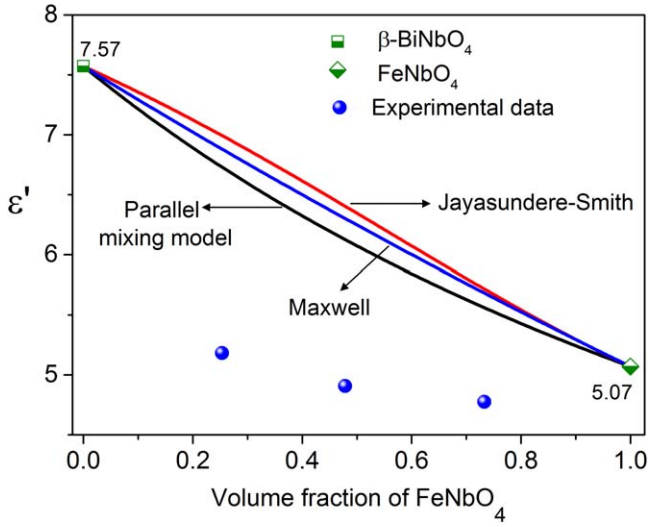

Figure 9. Dielectric constant of $(1-x)BiNbO_4$–$xFeNbO_4$ ceramics as a function of volume fraction of $FeNbO_4$: measured and calculated values.

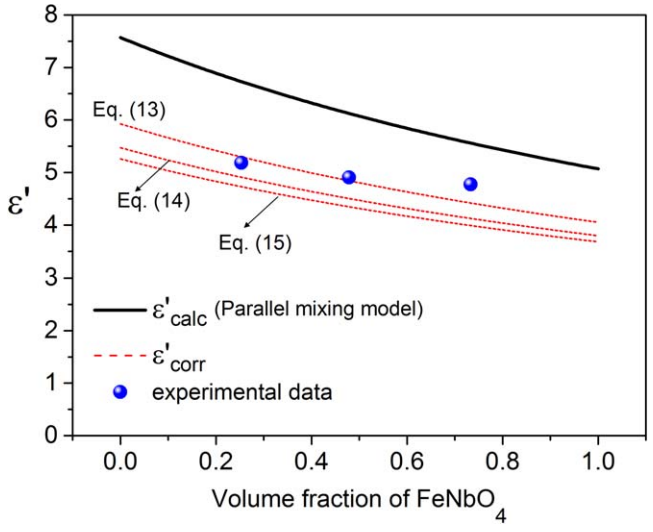

Figure 10. Dielectric constant of $(1-x)BiNbO_4$–$xFeNbO_4$ ceramics as a function of volume fraction of $FeNbO_4$: measured, predicted by the parallel mixing model and corrected considering the porosity of the samples.

Conclusions

A novel series of $(1-x)BiNbO_4$–$xFeNbO_4$ microwave dielectric ceramics was successfully prepared by the solid-state reaction method. The XRD analysis demonstrated that β-$BiNbO_4$ did not react with $FeNbO_4$ since no secondary phases were formed, proving the chemical compatibility between β-$BiNbO_4$ and $FeNbO_4$.

The experimental density of the prepared samples was about 75% of the theoretical density, even with low treatment temperature and without sintering aids, not compromising the mechanical strength of the binary system. The low treatment temperature allows the samples to co-fired with low melting point electrodes, such as Ag or Cu, which is an important requirement for some applications, and the absence of sintering aids avoided the formation of undesirable secondary phases.

The modified cavity perturbation technique was used to determine the dielectric properties of the studied materials, with the sample S1 showing the most promising characteristics, with dielectric losses lower than the ones presented by the precursors.

Table III. Dielectric properties: β-$BiNbO_4$ and $FeNbO_4$ phases and $(1-x)BiNbO_4$–$xFeNbO_4$ binary.

Precursors	**β-$BiNbO_4$**	**$FeNbO_4$**	
ε'	7.57	5.07	
ε''	0.12	0.45	
Q	1831	1823	
$BiNbO_4$–$FeNbO_4$	**S1**	**S2**	**S3**
V_2 ($FeNbO_4$) (%)	25.33	47.86	73.31
ε'_{exp}	5.18	4.91	4.77
ε'_{calc}	7.15	6.69	6.02
ε'_{corr}	5.19	4.88	4.43
ε''_{exp}	0.10	0.14	0.29
Q_{exp}	1747	1726	1657
Q_{calc}	1829	1827	1825

Different mixing laws were used to predict the dielectric constant of this binary system, with the parallel mixing model, corrected due to the porosity, presenting the best fitting to the measured values.

Acknowledgments

Susana Devesa acknowledges the post-doctoral grant under the project "SUSpENsE—CENTRO-01-0145-FEDER-000006." This work was partially supported by FEDER funds through the COMPETE 2020 Programme and National Funds through FCT—Portuguese Foundation for Science and Technology under the project UID/CTM/50025/2019.

ORCID

S. Devesa https://orcid.org/0000-0002-2217-4584

References

1. H. Chen, X. Fu, Q. An, B. Tang, S. Zhang, H. Yang, Y. Long, M. Harfouche, H. Wang, and Y. Li, "Determining the quality factor of dielectric ceramic mixtures with dielectric constants in the microwave frequency range." *Sci. Rep.*, **7**, 1 (2017).
2. D. Wang, S. Zhang, D. Zhou, K. Song, A. Feteira, Y. Vardaxoglou, W. Whittow, D. Cadman, and I. M. Reaney, "Temperature stable cold sintered $(Bi_{0.95}Li_{0.05})(V_{0.9}Mo_{0.1})O_4$-$Na_2Mo_2O_7$ microwave dielectric composites." *Mater.*, **12**, 1370 (2019).
3. C. Li, C. Yin, M. Deng, L. Shu, and J. Khaliq, "Tunable microwave dielectric properties in SrO-V_2O_5 system through compositional modulation." *J. Am. Ceram. Soc.*, **103**, 2315 (2020).
4. cf Tseng, H. C. Hsu, and P. H. Chen, "Microwave dielectric properties of $Li_2W_2O_7$ ceramics improved by Al_2O_3 addition." *J. Alloys Compd.*, **764**, 840 (2018).
5. S. Meng, Z. Yue, H. Zhuang, F. Zhao, and L. Li, "Microwave dielectric properties of $Ba_3(VO_4)_2$ -Mg_2SiO_4 composite ceramics." *J. Am. Ceram. Soc.*, **93**, 359 (2010).
6. B. Liu, C. C. Hu, Y. H. Huang, H. B. Bafrooei, and K. X. Song, "Crystal structure, infrared reflectivity spectra and microwave dielectric properties of $CaAl_2O_4$ ceramics with low permittivity." *J. Alloys Compd.*, **791**, 1033 (2019).
7. Y. Deng, P. Yao, and B. Li, "Crystal phase, microstructure and microwave properties of $Ba_2V_xO_7$ $(1.85 \leqslant x \leqslant 2.05)$ ceramics." *J. Mater. Sci., Mater. Electron.*, **31**, 7053 (2020).
8. A. Raveendran, M. T. Sebastian, and S. Raman, "Applications of microwave materials: a review." *J. Electron. Mater.*, **48**, 2601 (2019).
9. R. Hutcheon, M. de Jong, and F. Adams, "A system for rapid measurements of RF and microwave properties Up to 1400°C. Part1: theoritical development of the cavity frequency-shift data analysis equations." *J. Microw. Power Electromagn. Energy.*, **27**, 87 (1992).
10. J. Katrib, O. Folorunso, C. Dodds, G. Dimitrakis, and S. W. Kingman, "Improving the design of industrial microwave processing systems through prediction of the dielectric properties of complex multi-layered materials." *J. Mater. Sci.*, **50**, 7591 (2015).
11. S. Halder, S. Bhuyan, and R. N. P. Choudhary, "Structural, dielectric and electrical properties of bismuth magnesium tantalate electronic system." *J. Magnes. Alloy.*, **7**, 628 (2019).
12. N. A. Zhuk, S. M. Shugurov, M. G. Krzhizhanovskaya, V. A. Belyy, N. A. Sekushin, B. A. Makeev, S. V. Nekipelov, D. S. Beznosikov, and Y. A. Busargina, "The effect of CuO on the microstructure, spectral characteristics, thermal and electrical properties of $BiNbO_4$ ceramics." *J. Alloys Compd.*, **822**, 153619 (2020).
13. B. Huang, Y. Liu, Y. Lu, H. Gao, and H. Chen, "Structure and dielectric properties of Nd substituted $Bi_{1.5}MgNb_{1.5}O_7$ ceramics." *J. Mater. Sci., Mater. Electron.*, **24**, 2785 (2013).

14. K. Sudheendran and K. C. James Raju, "Electrical properties of pulsed laser deposited $Bi_2Zn_{2/3}Nb_{4/3}O_7$ thin films for high K gate dielectric application." *J. Mater. Sci., Mater. Electron.*, **22**, 626 (2011).
15. S. Devesa, M. P. Graça, and L. C. Costa, "Dielectric Characterization of (Bi1-xFe_x)NbO_4 Ceramics Prepared by Wet-Chemical Route." *Nanoscience and Nanotechnology in Security and Protection against CBRN Threats* (Springer, Dordrecht) p. 107 (2020).
16. X. Chen, D. Ma, G. Huang, G. Liu, and H. Zhou, "Structure and dielectric properties of a novel defect pyrochlore $Bi_{1.34}Fe_{0.66}Nb_{1.34}O_{6.35}$ ceramic." *J. Mater. Sci. Mater. Electron*, **27**, 8619 (2016).
17. E. Tuncer, Y. V. Serdyuk, and S. M. Gubanski, "Dielectric mixtures: electrical properties and modeling." *IEEE Trans. Dielectr. Electr. Insul.*, **9**, 809 (2002).
18. A. K. Jha and M. J. Akhtar, "A generalized rectangular cavity approach for determination of complex permittivity of materials." *IEEE Trans. Instrum. Meas.*, **63**, 2632 (2014).
19. S. Devesa, M. P. Graça, and L. C. Costa, "Structural, morphological and dielectric properties of $BiNbO_4$ ceramics prepared by the sol-gel method." *Mater. Res. Bull.*, **78**, 128 (2016).
20. S. Devesa, M. P. Graça, F. Henry, and L. C. Costa, "Dielectric properties of $FeNbO_4$ ceramics prepared by the sol-gel method." *Solid State Sci.*, **61**, 44 (2016).
21. N. Doebelin and R. Kleeberg, "Profex: a graphical user interface for the rietveld refinement program BGMN." *J. Appl. Cryst.*, **48**, 1573 (2015).
22. B. Muktha, J. Darriet, G. Madras, and T. N. G. Row, "Crystal structures and photocatalysis of the triclinic polymorphs of $BiNbO_4$ and $BiTaO_4$." *J. Solid State Chem.*, **179**, 3919 (2006).
23. E. Schmidbauer and J. Schneider, "Electrical resistivity, thermopower, and57Fe mössbauer study of $FeNbO_4$." *J. Solid State Chem.*, **134**, 253 (1997).
24. M. J. Iqbal, M. N. Ashiq, and I. H. Gul, "Physical, electrical and dielectric properties of Ca-substituted strontium hexaferrite ($SrFe_{12}O_{19}$) nanoparticles synthesized by co-precipitation method." *J. Magn. Mater.*, **322**, 1720 (2010).
25. K. Yi, D. Geng, C. Shang, Y. He, and J. Yang, "The application of thermogravimetric analysis method in the determination of aramid fiber content in composite ICCST/10." *10th International Conference on Composite Science and Technology* (2015), http://dem.ist.utl.pt/iccst10/files/ICCST10_Proceedings/pdf/WEB_PAPERS/ICCST10_Upload_94.pdf.
26. R. J. Meredith, *Engineers' handbook of industrial microwave heating, institution of electrical engineers* (Institution of Electrical Engineers, United Kingdom) 25, p. 310 (1998), IEE Power Series.
27. S. Balmus, G. Pascariu, F. Creanga, I. Dumitru, and D. D. Sandu, "The cavity perturbation method for the measurement of the relative dielectric permitivity in the microwave range." *J. Optoelectron. Adv. Mater.*, **8**, 971 (2006).
28. L. C. Costa, S. Devesa, and F. Henry, "A 5 GHz resonant cavity for complex permittivity measurements: design, test performances and application." *Mater. Sci. Forum*, **514**, 1561 (2006).
29. S. J. Penn, N. M. Alford, A. Templeton, X. Wang, M. Xu, and M. Reece, "Effect of porosity and grain size on the microwave dielectric properties of sintered alumina." *J. Am. Ceram. Soc.*, **80**, 1885 (1997).
30. M. Lanagan, J. Guo, and C. Randall, "Effect of porosity and microstructure on the microwave dielectric properties of rutile." *Mater. Lett.*, **200**, 101 (2017).